Synchrotron Computed Microtomography of Porous Media: Topology and Transports

P. Spanne,[1] J. F. Thovert,[2] C. J. Jacquin,[3] W. B. Lindquist,[4] K. W. Jones,[1] and P. M. Adler[2]

[1]*Brookhaven National Laboratory, Upton, New York 11973*

[2]*Laboratoire des Phénomènes de Transport dans les Mélanges, Asterama 2, Avenue du Téléport, 86360- Chasseneuil, France*

[3]*Institut Français du Pétrole, BP 311, 92506, Rueil-Malmaison, France*

[4]*State University of New York, Stony Brook, New York 11794*

(Received 9 November 1993)

Computed microtomography is applied to a piece of Fontainebleau sandstone in order to determine the geometrical structure of the pores. The topology of the void space is then derived from the tomographic image of the volume. Permeability and conductivity are computed and found in good agreement with experimental data. Perspectives offered by this new nondestructive method with a potential resolution of the order of one micrometer or less are analyzed.

PACS numbers: 87.59.Fm, 44.30.+v, 47.55.Mh, 61.43.−j

1. Introduction.—Determination of the macroscopic properties of porous materials is a longstanding problem of great interest, for instance for the oil industry [1]. This determination necessitates two steps; the geometry of real materials must be adequately described, following which the local field equations must be solved [2]. Given the availability of high-speed computers, the geometrical step is the more difficult of the two. In the last fifty years, there has been an intensive search of realistic geometries [2], such as the recent method of reconstructed media [2,3]. Experimental determination of detailed pore structure by a classical method such as impregnation by epoxy resin is tedious though it may yield interesting two-dimensional informations on thin sections [4]. The obtention of the three-dimensional data by serial sectioning is still much more difficult [3,5].

The major purpose of this paper is to report on application of synchrotron computed microtomography (CMT) to the study of real porous media. Section 2 presents microtomography and the geological porous medium which is used. The genus of the pore space is determined in Sec. 3. Conductivity and permeability are analyzed in Sec. 4. All these quantities are successfully compared to independent estimations. General comments on the potential of this new method are given in the final section.

2. Experimental methods.—Fontainebleau sandstones are usually selected for first measurements because they are known to be remarkably homogeneous for geological materials [6]. A family of 94 cylindrical plugs with 4 cm diam and 4 cm high was collected [6]. The samples could be classified into three groups, according to their porosity. Twenty plugs were found in the central group with a porosity, $\mathcal{E}$, equal to 0.197 and a permeability $K_{\text{exp}} = 1860$ mD (1 Darcy $= 10^{-12}$ m^2).

In porous materials, at each point $\mathbf{x}$ within the sample, one can define a phase function $Z(\mathbf{x})$ which is equal to 1 if $\mathbf{x}$ belongs to the pore space V_L and 0 otherwise. Since the following analysis is restricted to statistically homogeneous media, the porosity, $\mathcal{E}$, can be defined by the statistical average

$$\mathcal{E} = \overline{Z(\mathbf{x})}. \tag{1}$$

The experimental work on CMT was performed at the Brookhaven National Synchrotron Light Source X26 beam line. The experimental arrangement has been described previously [7]. Briefly, a pencil beam of x rays is formed by using a collimator with a fixed opening. In the present work it was 5 μm wide and 5 μm high. The tomographic sections were obtained using a first generation rotate-translate method. The x rays transmitted through the sample are detected using a scintillation counter operated in current mode. The primary x-ray beam from the X26 bending magnet source was filtered with a 100 μm thick Mo foil to obtain an x-ray energy spectrum with a full width at half maximum of about 10 μm and a mean energy of roughly 19 keV. The pixel size was 10 μm $\times$10 μm and the distance in the reconstructed images between consecutive tomographic sections was 10 μm. A volume image of the Fontainebleau sandstone was obtained by making 100 sequential tomographic sections.

The image matrix size for each section was 303 $\times$ 303 elements. Only a limited image of the pore structure in a volume 60 $\times$ 60 $\times$ 60 voxels at the center of the sandstone is shown in Fig. 1. It can be usefully compared to the pictures derived from serial sectioning of Vosges sandstones [3].

From the original data of 303 $\times$ 303 $\times$ 100 voxels, the largest parallelepipedic domain V entirely contained within the sandstone was retained. This corresponds to the files of integers $\{Z(i,j,k);\ i = 1, N_{cx};\ j = 1, N_{cy};\ k = 1, N_{cz}\}$ with $N_{cx} = 121$, $N_{cy} = 161$, $N_{cz} = 100$. Five cubic subdomains $V_{Li} (i = 1, \ldots, 5)$ of the total domain V were used for the computations; the coordinates of the center of gravity and the size N_c of each subdomain are given in pixels in Table I.

3. Topology.—The major purpose of topology is to characterize the structure of a porous medium by a few intrinsic parameters [5]. Put inside each pore of a

0031-9007/94/73(14)/2001(4)$06.00

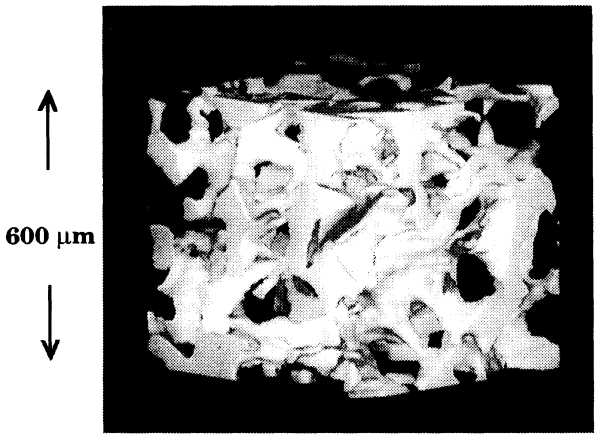

FIG. 1. Views of the pore space of Fontainebleau sandstones obtained by CMT. The pore structure is shown as white and the rock as black. That is, the pore structure is opaque and the rock transparent.

porous medium a single pipe (or wirelike an electrical wire); hence the medium can be viewed as a set of interconnected pipes called the graph **G** of the pore space. **G** can be determined by a progressive conditional thinning of the pore space [8].

In the numerical computations relative to the subdomains V_{Li} $(i = 1,\ldots,5)$, additional margins were added to the sample [Fig. 2(a)], in order to prevent pores crossing the volume boundaries from being eroded when extracting the graph. An empty slit was set along each face of the parallelepiped. Impermeable boundaries were also introduced along the y and z directions. These boundary conditions might introduce some artifacts in the peripheral zone of the volume, which should become negligible when the size of the volume is increased. β_i^1 is equal to the number of independent cycles of the graph and is called the cyclomatic number or the genus

$$\beta_i^1 = m_i - n_i + 1, \qquad (2)$$

where m_i and n_i are the number of edges and vertices in the volume V_{Li}. For a statistically homogeneous medium, it is more appropriate to introduce the number $\beta_i'^1$ of cycles per unit volume. $\beta_i'^1$ characterizes the connectivity of the pore space, i.e., it measures the number of independent paths between two points within the pore space, or, equivalently the degree to which it is multiply connected. Though $\beta_i'^1$ helps to define the geometry of the pore space and thus generated a lot of interest [5,9], its relation to the macroscopic transport properties is not direct; for instance, permeability is certainly a function of $\beta_i'^1$, but is also proportional to the square of a characteristic length, information which is not contained in $\beta_i'^1$.

The intrinsic numbers $\mathcal{E}$ and $\beta_i'^1$ displayed in Table I are relatively constant if one excepts V_{L1}. This fluctuation for V_{L1} might be due to the small size of the sample; such statistical fluctuations are expected, since the order of magnitude of the size of the grains which compose these sandstones is 250 μm.

Another important interest of the $\beta_i'^1$ is that they are successfully compared to the values obtained for reconstructed media based on Fontainebleau sandstones [8] for similar porosities. $\beta_i'^1$ was found equal to 830, 570, and 1750, for samples with porosities $\mathcal{E} = 0.14$, 0.209, and 0.28, respectively. Results obtained on Berea sandstones [9] are in fair agreement with these data since $\beta_i'^1$ is equal to 520. One could take into account the correlation lengths to improve these comparisons.

Finally, the graph themselves are presented in Fig. 3. In order to remove some unrealistic features occurring in a peripheral layer as a consequence of the arbitrary boundary condition assumed in the computation, a superficial layer of two voxels has been removed all around the volume [see Fig. 2(a)]. Qualitatively, these graphs compare very well with the ones obtained for reconstructed porous media [8]. It should be noticed how useful these graphs are to schematize the structure of porous media, even when the porosity is approximately equal to 20%; this structure is indeed difficult to grasp on the 3D tomogram itself (Fig. 1).

4. Formation factor and permeability.—The simplest macroscopic property of a porous medium is its macroscopic conductivity $\overline{\sigma}$. The formation factor F is usually defined as the inverse of the dimensionless relative electrical conductivity $\overline{\sigma}/\sigma_0$ of a porous medium filled by a conducting liquid phase of conductivity σ_0. In order to determine F, one has to solve the Laplace equation in samples of reconstructed media with no flux at the solid walls and with periodic boundary conditions at the surface

TABLE I. Topological characteristics and macroscopic transport properties of samples V_{Li} $(i = 1,\ldots,5)$ of the pore space obtained with CMT.

Volume	Size N_c	Coordinates of the center	Porosity	Formation factors F_0	$F_{\min}$	$F_{\max}$	Archie's law (4)	Permeability K_{cal} (mD) $M = 1$	$M = 8$	$\beta_i'^1$ mm^{-3}
V_{L1}	44^3	60, 79, 48	0.211	26	17	19	16	2100	3000	1080
V_{L2}	64^3	60, 79, 48	0.185	42	25	27	20	1400	1700	858
V_{L3}	84^3	60, 79, 48	0.179	36	26	28	21	1330	1600	812
V_{L4}	44^3	30, 30, 30	0.174	54	43	48	22	580	610	822
V_{L5}	54^3	35, 35, 35	0.186	43	36	41	20	770	810	895

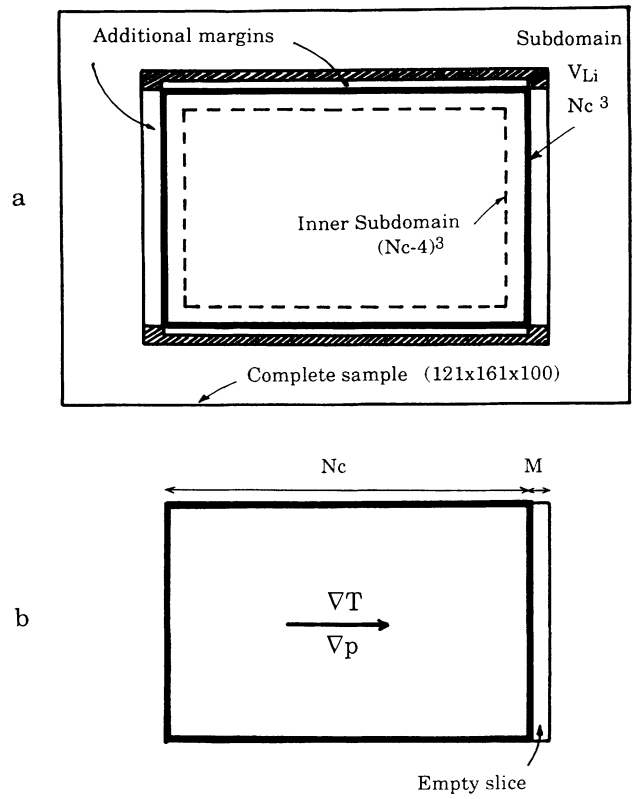

FIG. 2. Definitions of the boundary conditions. Subdomains V_{Li} (N_c^3, heavy solid line) were cut out of the complete sample V ($121 \times 161 \times 100$, solid line). (a) When the graph is extracted, the additional margins are added. The graphs displayed in Fig. 3 correspond to the inner subdomains $(N_c - 4)^3$, dashed line. During the resolution of the transport problems, an additional slice of length M is added to the volume V_{Li} (b).

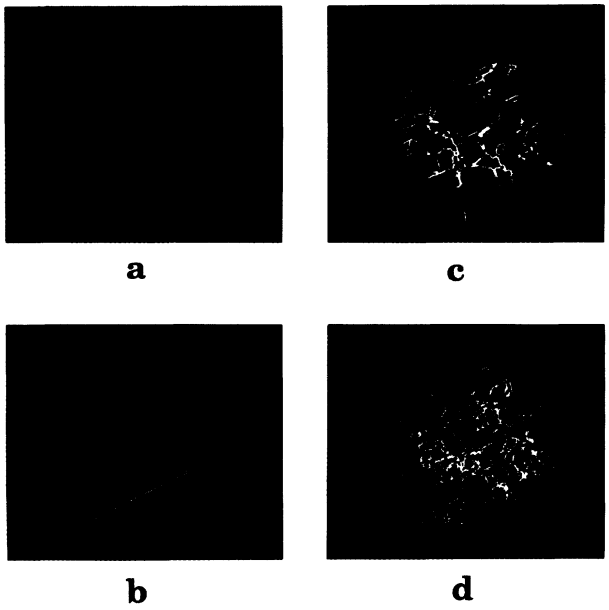

FIG. 3. Visualization of the pore spaces (a),(b) and of the corresponding graphs (c),(d) in the concentric samples V_{L1} and V_{L2}. The pore space is green and the rock is black (and transparent as in Fig. 1). Only the inner subdomains sketched in Fig. 2(a) are displayed. Note that the scales are different; the size of the cube is 400 μm (a),(c); 600 μm (b),(d). The edges and vertices of the graphs are yellow and red, respectively.

of the unit cell [10]. The accuracy of the numerical calculations in complex 3D domains has been checked [10] and it was found to be of the order of 5%. Similar computations have been recently performed [11], but they were applied to model media instead of real ones as here.

Three different values are given in Table I for conductivity because of the overall spatially periodic boundary condition. If the sample is used directly, the pores located on opposite faces of the unit cell do not coincide; the corresponding value for the formation factor is denoted by F_0. It is believed to give an upper limit for the formation factor. Other values can be tentatively obtained by the following operations. Spatially periodic boundary conditions are applied, but the sample is supplemented with a slice of length M between two successive cells in the direction of the average potential gradient [Fig. 2(b)]. This is made in order to enforce continuous paths in the pore space which cross the sample boundary. The conductivity C of the slice is either 1 or ε. The resolution of the Laplace equation yields an apparent conductivity σ_{app} from which an actual value F_{app} can be deduced

$$F_{\text{app}} = (N_c + M - \sigma_{\text{app}}/C)/N_c\sigma_{\text{app}} . \quad (3)$$

Alternatively, constant temperatures can be imposed on the two opposite faces of the sample with a jump ΔT.

In Table I, the minimal and maximal values F_{min} and F_{max} obtained with these various schemes with M ranging from 1 to 16 are listed; the precision of the approximations involved in (3) is pretty good.

Because of the remarkable homogeneity of Fontainebleau sandstones, the numerical results can be compared with experimental data [10] obtained on different samples. These data are well correlated by Archie's law [2]

$$F_{\text{exp}} = k\mathcal{E}^{-m} \quad (4)$$

with a cementation factor $m = 1.64$ and a constant $k = 1.27$. The comparison is made in Table I. It is seen that the agreement between the calculated and the measured formation factor F_{exp} is good to within a factor of 2.

Let us now consider the flow of an incompressible Newtonian fluid at low Reynolds number which is governed by the Stokes equations with the no slip condition at the wall [2]. The seepage velocity $\overline{v}$ is a linear function of the macroscopic pressure gradient $\nabla\bar{p}$.

$$\overline{v} = -\left(\frac{1}{\mu}\right)\mathbf{K} \cdot \nabla\bar{p} . \quad (5)$$

Here only the component K_{xx} of the permeability **K** has been computed. Again because of the same problem of adequate overall boundary conditions, an empty slice of length M has been added to the sample on one of the external faces normal to the average flow direction. This addition has two effects; it influences the flow in the porous sample (and thus the value of K_{xx} itself) and also the flow in the slice. If these effects are assumed to be negligible, one has

$$K_{\mathrm{cal}} = K_{xx} N_c/(N_c + M). \quad (6)$$

Because of the length of the computations, permeability was only computed for $M = 1$ and 8 (see Table I). Except for V_{L1}, the relative difference between these two values is smaller than 10%; again this provides an order of magnitude for the precision of the approximations involved in (6). These values of K can be directly compared with the experimental data $K_{\mathrm{exp}} = 1860$ mD for the same set of samples. The agreement is reasonable. Note that these results are consistent also with the ones found for the formation factor in the sense that the permeability and the formation factor should vary in opposite ways. The fluctuations can again be attributed to the relatively small size of the samples when compared to the average size of the solid grains which compose the sandstones.

One of the major problems which had severely slowed down the pace of research in domains like porous media is the fact that the geometrical influence is crucial and that it was very hard to get detailed information on it. A tool like CMT is essential for further studies of porous media, since the geometry can be obtained with great accuracy and relatively small efforts for the analysis of an extra sample when the whole machinery has been set up.

Moreover, tomograms are delivered in a digital format for further use by computer routines which are able to calculate the macroscopic properties of the samples. The applications which have been presented in this paper show that the results of these routines are in satisfactory agreement with measurements (though they were not obtained on the same samples).

Three major paths of development can be foreseen along these lines. In industrial applications, a CMT measurement may generate input to a number of programs which will provide overnight a number of macroscopic properties. The cost of these computations is lower than the one of the corresponding experimental measurements. These computations will be of particular value for properties which are delicate to measure. Moreover the evolution of certain properties (because of deposition [12] for instance) can be predicted in a short time, even though the measurements are necessarily long.

The second path of development is the study of the random geometry of real porous media. The characterization of such geometries is of a high theoretical and practical interest.

The last path concerns the tools themselves. On one hand, CMT with an even better resolution can certainly be envisioned and would open up further areas of research, such as media with micro and macro porosities [2]. On the other hand, more efficient numerical routines, specifically development of algorithms for parallel computers, can be conceived to calculate the properties of these media.

This work was supported in part by the U.S. Department of Energy under Contract No. DE-AC02-76CH00016 (K. W. J., P. S.) and the Swedish Natural Science Research Council under Grant No. 8273-306 (P. S.). The Fontainebleau samples were kindly prepared by B. Zinszner (I. F. P.).

[1] A. J. Katz and A. H. Thompson, Phys. Rev. B **34**, 8179 (1986); A. H. Thompson, A. J. Katz, and R. A. Raschke, Phys. Rev. Lett **58**, 29 (1986).

[2] P. M. Adler, *Porous Media: Geometry and Transports* (Butterworth/Heinemann, Stoneham, 1992); F. A. L. Dullien, *Porous Media: Fluid Transport and Pore Structure* (Academic Press, New York, 1979).

[3] J. Yao, P. Frykman, F. Kalaydjian, J. F. Thovert, and P. M. Adler, J. Colloid. Interface Sci. **156**, 478 (1993).

[4] J. G. Berryman and S. C. Blair, J. Appl. Phys. **60**, 1930 (1986).

[5] C. Lin and M. H. Cohen, J. Appl. Phys. **53**, 4152 (1982).

[6] B. Zinszner and C. Meynot, Rev. Inst. Fr. **37**, 337 (1982); N. Lucet, Ph.D. thesis, Université de Paris VI, 1989.

[7] P. Spanne, K. W. Jones, H. Herman, and W. L. Riggs, J. Thermal Spray Technology **2**, 121 (1993).

[8] J. F. Thovert, J. Salles, and P. M. Adler, J. Microscopy **170**, 65 (1993).

[9] I. F. MacDonald, P. M. Kaufmann, and F. A. L. Dullien, J. Microsc. **144**, 297 (1986).

[10] C. G. Jacquin, Rev. Inst. Fr. Pet. **19**, 921 (1964); P. M. Adler, C. G. Jacquin, and J. F. Thovert, Water Res. Res. **28**, 1571 (1992); J. F. Thovert, F. Wary, and P. M. Adler, J. Appl. Phys. **68**, 3872 (1990).

[11] L. M. Schwartz, N. Martys, D. P. Bentz, E. J. Garboczi, and S. Torquato, Phys. Rev. E **48**, 4584 (1993).

[12] J. Salles, J. F. Thovert, and P. M. Adler, Chem. Eng. Sci. **48**, 2839 (1993).

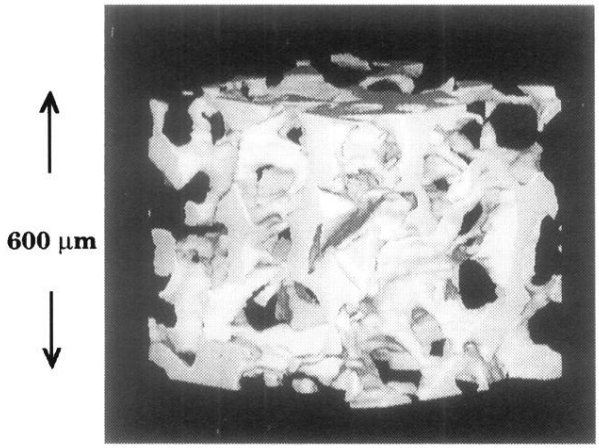

FIG. 1. Views of the pore space of Fontainebleau sandstones obtained by CMT. The pore structure is shown as white and the rock as black. That is, the pore structure is opaque and the rock transparent.

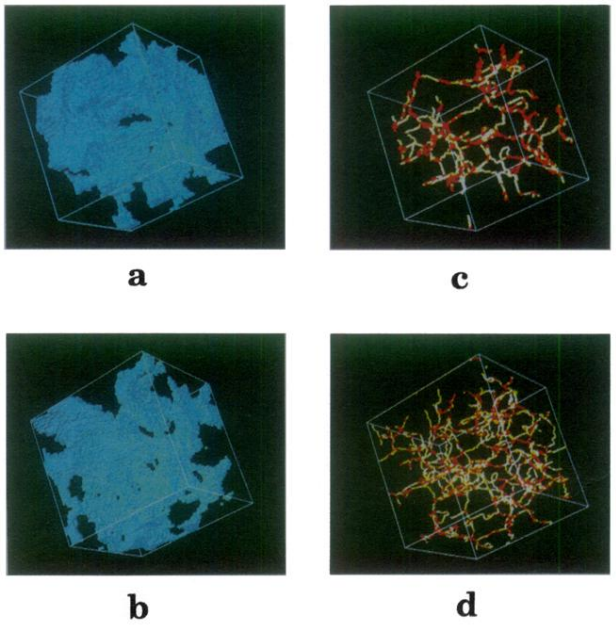

FIG. 3. Visualization of the pore spaces (a),(b) and of the corresponding graphs (c),(d) in the concentric samples V_{L1} and V_{L2}. The pore space is green and the rock is black (and transparent as in Fig. 1). Only the inner subdomains sketched in Fig. 2(a) are displayed. Note that the scales are different; the size of the cube is 400 μm (a),(c); 600 μm (b),(d). The edges and vertices of the graphs are yellow and red, respectively.